Mineralogical Magazine, November 2014, Vol. 78(6), pp. 1449–1464

OPEN ACCESS

An experimental study of tremolite dissolution rates as a function of pH and temperature: Implications for tremolite toxicity and its use in carbon storage

TAMARA DIEDRICH[1,§], JACQUES SCHOTT[1] AND ERIC H. OELKERS[1,2,*]

[1] GET-Université de Toulouse-CNRS-IRD-OMP, 14 Avenue Edouard Belin, 31400 Toulouse, France
[2] Earth Sciences, University College London, Gower Street, London WC1E 6BT, UK

[*Received 12 August 2014; Accepted 9 November 2014; Associate Editor: T. Stawski*]

ABSTRACT

Steady-state tremolite dissolution rates, at far-from-equilibrium conditions, were measured as a function of aqueous silica and magnesium activity, pH from 1.9 to 6.7, and temperature from 25 to 150ºC. Calcium is released from tremolite faster than either Mg or Si throughout most of the experiments even after these latter elements attained steady-state release rates. The preferential removal of Ca releases fine Mg-Si rich needle-like fibres from the tremolite, probably promoting its toxicity. In contrast, Mg was released in stoichiometric or near to stoichiometric proportion to Si once steady-state was attained. Measured steady-state tremolite dissolution rates based on Si release can be described using

$$r_+ = \left(A_A \left(\frac{a_{H^+}^2}{a_{Mg^{2+}}} \right)^{1/8} \right) \exp(E_A/RT)$$

where r_+ signifies the BET surface area-normalized forward tremolite steady-state dissolution rate, A_A refers to a pre-exponential factor = 6×10^{-3} mol cm^{-2} s^{-1}, E_A designates an activation energy equal to 80 kJ mol^{-1}, R represents the gas constant, T denotes absolute temperature, and a_i refers to the activity of the subscripted aqueous species. This rate expression is consistent with tremolite dissolution rates at acidic pH being controlled by the detachment of partially liberated silica tetrahedra formed from the exchange of Mg^{2+} for two protons near the mineral surface after the near-surface Ca has been removed. Nevertheless, Mg release rates from tremolite are ~3 orders of magnitude slower than those from forsterite and enstatite suggesting that tremolite carbonation will be far less efficient than the carbonation of these other Mg-silicate minerals.

KEYWORDS: tremolite, dissolution rates, biodurability, mineral carbonation.

Introduction

THIS work is part of a systematic study aimed at the characterization of Mg-silicate mineral dissolution rates. A significant number of past studies have focused on the dissolution rates of the divalent metal silicates, including studies of the dissolution rates of forsterite (Murphy and Helgeson, 1987, 1989; Wogelius and Walther, 1991, 1992; Pokrovsky and Schott, 2000; Rosso

* E-mail: Oelkers@get.obs-mip.fr
§ Present address: Barr Consulting, Duluth MN, USA
DOI: 10.1180/minmag.2014.078.6.12

This paper is published as part of a special issue in *Mineralogical Magazine*, Vol. **78(6)**, 2014 entitled 'Mineral–fluid interactions: scaling, surface reactivity and natural systems'.

and Rimstidt, 2000; Oelkers, 2001b; Golubev *et al*., 2005; Olsen and Rimstidt, 2008; Prigiobbe e*t al.* 2009; Daval *et al.*, 2011*a*; King *et al.*, 2014), enstatite (Schott *et al.*, 1981; Oelkers and Schott, 2001), diopside (Petit *et al*., 1987; Knauss *et al.*, 1993; Brantley and Chen, 1995; Chen and Brantley, 1998; Golubev *et al.*, 2005; Golubev and Pokrovsky, 2006; Dixit and Carroll, 2007; Daval *et al.*, 2011*b*, 2013) and talc (Lin and Clemency, 1981; Jurinski and Rimstidt, 2001; Saldi *et al.*, 2007).

The motivation for this study is several fold:

(1) The dissolution rates of Ca- and Mg-bearing silicates, such as tremolite, are of particular interest as they are potential sources of the divalent metals required for the mineralogical storage of CO_2 (cf. Oelkers and Schott, 2005; Hänchen *et al*., 2008; Oelkers and Cole, 2008; Oelkers *et al*., 2008*a*; King *et al*., 2010; Ryu *et al*., 2011; Saldi *et al*., 2012; Gislason and Oelkers, 2014).

(2) Exposure to tremolite is widely recognized as a cause of asbestos-related diseases (Churg, 1988; Case, 1991; Davis *et al*., 1991; Robledo and Mossman, 1999; Roggli *et al.*, 2002; Gunter *et al*., 2007; Pugnaloni *et al*., 2013). A particle's ability to resist dissolution once submerged in lung fluid (i.e. its biodurability) may be a critical determinant in its toxicity (Addison and McConnell, 2008). This connection has motivated several previous studies aimed at quantifying tremolite biodurability (Oze and Solt, 2010; Rozalen *et al*., 2013).

(3) The dissolution rates of the Mg silicates appear to exhibit a systematic behaviour as a function of aqueous solution pH and composition (Schott *et al*., 2009). It is anticipated that this study will provide further insight into this systematic behavior of these minerals.

The goal of this study is to expand our knowledge of tremolite dissolution kinetics at acid to neutral pH. Thus tremolite dissolution rates have been measured at 25 to 150ºC, and $1.9 < pH < 6.7$ as a function of aqueous fluid concentration at far-from-equilibrium conditions. The results of this study illuminate the durability of tremolite at conditions relevant to mineral carbonation and human health.

To date there have been relatively few studies of the dissolution rates of tremolite reported in the literature. Schott *et al*. (1981) reported the dissolution rates of tremolite at 22ºC at $1 \leqslant pH \leqslant 6$ in aqueous HCl solutions measured in batch reactors. Mast and Drever (1987) reported the dissolution rates of tremolite at 22ºC and $2 \leqslant pH \leqslant 9$ in aqueous solutions containing HCl, $KHCO_3$, H_3BO_3 and KOH measured in fluidized bed reactors. Measured rates decrease slightly with increasing pH to at least pH 9. In addition, both of these experimental studies observed a preferential release of Mg over Si during the early stages of experiments performed at acidic conditions prior to attainment of stoichiometric steady-state dissolution. This behaviour and similar observations on other divalent metal silicates reported by Oelkers *et al*. (2009) were attributed to a relatively rapid exchange reaction between H^+ and Mg^{2+} on the mineral surfaces. Similarly, Schott *et al*. (1981) reported that Ca was preferentially released compared to both Mg and Si during tremolite dissolution at acid conditions. Mast and Drever (1987) performed additional tremolite dissolution experiments at pH 4 and 7 as a function of aqueous oxalate concentrations. In contrast to the effect of the presence of aqueous organic species on Al-silicate minerals (cf. Oelkers and Schott, 1998), no effect of the presence of aqueous oxalate was observed for oxalate concentrations $\leqslant 10^{-3}$ M. The present study expands upon this past work by determining tremolite steady-state dissolution rates over a wide range of pH at temperatures between 25 and 150ºC and by establishing an equation to describe these rates over a variety of environmental conditions.

Theoretical background

The standard state adopted in this study is that of unit activity for pure minerals and H_2O at any temperature and pressure. For aqueous species other than H_2O, the standard state is unit activity of the species in a hypothetical 1 molal solution referenced to infinite dilution at any temperature and pressure. Tremolite dissolution can be described according to:

$$Ca_2Mg_5Si_8O_{22}(OH)_2 + 14H^+ \rightleftharpoons 2Ca^{2+}\ 5Mg^{2+} + 8SiO_2\ (aq) + 8H_2O \qquad (1)$$

Note that SiO_2(aq) in reaction 1 represents the H_4SiO_4 neutral aqueous species rather than total dissolved Si. Taking account of the standard state, the law of mass action for reaction 1 can be written

$$K_{tremolite} = a^2_{Ca^{2+}} a^5_{Mg^{2+}} a^8_{SiO_2(aq)} a^{-14}_{H^+} \qquad (2)$$

where $K_{tremolite}$ stands for the equilibrium constant of reaction 1, and a_i represents the activity of the subscripted aqueous species. The

https://doi.org/10.1180/minmag.2014.078.6.12 Published online by Cambridge University Press

chemical affinity (A) for reaction 1 can be expressed as

$$A = \mathrm{R}T \ln \left(\frac{a^2_{\mathrm{Ca}^{2+}} a^5_{\mathrm{Mg}^{2+}} a^8_{\mathrm{SiO_2(aq)}}}{K_{\mathrm{tremolite}} a^{14}_{\mathrm{H}^+}} \right) \qquad (3)$$

where R designates the gas constant, and T represents absolute temperature. When the fluid is undersaturated with respect to tremolite, A is negative, and when the fluid is supersaturated, A is positive. All thermodynamic calculations reported in the present study were performed using the *PHREEQC* 2.6 computer code (Parkhurst and Appelo, 1999) together with its llnl database (Johnson *et al.*, 2000). It is assumed in all thermodynamic calculations that the solid used in the dissolution experiments was pure stoichiometric tremolite. Although surface complexation theory suggests that the activities of charged particles on charged surfaces may differ somewhat from unity (Davis and Kent, 1990), the activities of species at the tremolite surface are assumed to be equal to their mole fraction. This latter assumption is shown below to be consistent with measured rate data.

Within the context of Transition State Theory, surface reaction-controlled dissolution rates can be considered to be the difference between the forward rate (r_+) and the reverse rate (r_-) such that

$$r = r_+ - r_- = r_+ \left(1 - \frac{r_-}{r_+} \right) \qquad (4)$$

Taking account of the law of detailed balancing it can be shown that equation 4 is equivalent to (Aagaard and Helgeson, 1977, 1982; Lasaga, 1981; Schott and Oelkers, 1995)

$$r = r_+(1 - \exp(-A/\sigma \mathrm{R}T)) \qquad (5)$$

where σ stands for Temkin's average stoichiometric number equal to the ratio of the rate of destruction of the activated or precursor complex relative to the overall dissolution rate. The form of equation 5 is such that overall rates (r) equal forward rates (r_+) when $A >> \sigma \mathrm{R}T$. All dissolution rates in the present study were measured at far-from-equilibrium conditions, such that $A >> \sigma \mathrm{R}T$. At these conditions $r_- << r_+$ and thus $r \approx r_+$. Tremolite dissolution rates in this study are thus symbolized r_+. Such experimental results can be used to assess the effect of aqueous solution composition on forward dissolution rates independently of the effects of chemical affinity.

Steady-state forward tremolite dissolution rates in this study are quantified using the multi-oxide silicate dissolution model of Oelkers (2001*a*). Within this model, dissolution proceeds *via* the sequential breaking of metal–oxygen bonds until the mineral structure is destroyed. The tremolite structure consists of Ca–O and Mg–O bonds in 8-fold and 6-fold coordination, respectively, and tetrahedral Si–O bonds (Hawthorne and Oberti, 2007). Silicon tetrahedra form double chains layered between strips of edge-sharing octahedra. In accord with Oelkers (2001*a*) and consistent with the results reported below, the relative rate of breaking these bonds are Ca–O > Mg–O > Si–O. This conclusion is consistent with the observations that Mg and Ca are initially released more rapidly than Si from divalent metal silicates (e.g. Luce *et al.*, 1972; Lin and Clemency, 1981; Schott *et al.*, 1981; Berner and Schott, 1982; Petit *et al.*, 1987; Oelkers and Schott, 2001; Oelkers *et al.*, 2009). Such observations suggest that the tremolite dissolution mechanism is initiated by the relatively rapid removal of Ca atoms and Mg atoms *via* Ca-H and Mg-H exchange reactions (Oelkers, 2001*a*). This exchange reaction partially liberates Si-O tetrahedra, which are subsequently released to aqueous solution, completing the dissolution process. In accord with transition state theory, far-from-equilibrium tremolite dissolution rates will therefore be proportional to the concentration of partially detached Si-tetrahedra (cf. Oelkers 2001*a*; Schott *et al.*, 2009) such that

$$r_+ = \mathrm{k}_+[> Si^*] = \mathrm{k}_+ \prod_i \left(\frac{\mathrm{K}_i \left(\frac{a^{z_i}_{\mathrm{H}^+}}{a^{z_i^+}_{\mathrm{M}_i^{z_i}}} \right)^{1/n}}{1 + \mathrm{K}_i \left(\frac{a^{z_i}_{\mathrm{H}^+}}{a^{z_i^+}_{\mathrm{M}_i^{z_i}}} \right)^{1/n}} \right) \qquad (6)$$

In equation 6 [$> Si^*$] represents the concentration of partially detached Si tetrahedra at the tremolite surface, k_+ designates a rate constant, a_i again refers to the activity of the subscripted aqueous species, M_i and z_i stand for the identity and the charge of the cations exchanged with protons to create the partially liberated Si tetrahedra (in the case of tremolite, $\mathrm{M}_i^{z_i}$ refers to Ca^{2+} and Mg^{2+}), n denotes a stoichiometric coefficient equal to the number of partially detached Si tetrahedra formed by the removal of each divalent cation, and K_i designates the equilibrium constant for the metal–proton exchange reactions. Note that the product on

https://doi.org/10.1180/minmag.2014.078.6.12 Published online by Cambridge University Press

the right hand side of equation 6 calculates the concentration of partially detached Si tetrahedra forming due to proton−metal exchange reactions. In cases where all of one type of cation is removed from the mineral surface, the parenthetical term on the right side of equation (6) reduces to unity; in cases where there are relatively few of one type of cations removed from the surface, this parenthetical term reduces to (see Oelkers and Schott, 2001):

$$\mathrm{K}_i \left(\frac{a_{\mathrm{H}^+}^{z_i^+}}{a_{\mathrm{M}_i}^{z_i^+}} \right)$$

In the case of tremolite at the conditions considered in the present study, Ca is removed rapidly from the mineral surface and continues to be removed ~6 times more rapidly, when normalized for its stoichiometry, than either Mg or Si even after these latter two elements attain a steady-state release rate. Magnesium, in contrast, is released in close-to-stoichiometric quantities compared to Si at steady-state (see below). In such cases equation 6 reduces to (see Oelkers, 2001*a*; Oelkers and Schott, 2001; Saldi *et al*., 2007)

$$r_+ \approx k'_+ \left(\frac{a_{\mathrm{H}^+}^2}{a_{\mathrm{Mg}^{2+}}} \right)^{1/n} \quad (7)$$

where k'_+ refers to the product $k_+\mathrm{K}_{\mathrm{Mg}}$. This equation suggests that increasing aqueous hydrogen ion activity and decreasing aqueous Mg activity will increase far-from-equilibrium tremolite dissolution rates and these rates will be independent of aqueous Si activity.

The variation in rate constants with temperature is commonly described using an Arrhenius equation such as (Arrhenius, 1889):

$$k'_+ = A_{\mathrm{A}} e^{-\left(\frac{E_{\mathrm{A}}}{\mathrm{R}T}\right)} \quad (8)$$

where A_{A} stands for a pre-exponential factor, E_{A} is the activation energy, R refers to the gas constant and T signifies the absolute temperature. Combining equations 7 and 8 gives an equation describing tremolite forward dissolution rates with respect to the temperature and aqueous solution composition:

$$r_+ \approx A_{\mathrm{A}} \exp(-E_{\mathrm{A}}/\mathrm{R}T) \left(\frac{a_{\mathrm{H}^+}^2}{a_{\mathrm{Mg}^{2+}}} \right)^{1/n} \quad (9)$$

The degree to which equation 9 provides a quantitative description of tremolite dissolution rates is assessed below.

Methods and samples

Two different tremolite samples were used in this study, providing some variation in tremolite morphology in the starting material. One sample (tremolite A) was a massive sample of bladed to prismatic tremolite crystals from Felch, Michigan, USA, and the other (Tremolite B) was a fibrous tremolite sample from Cannan, Connecticut, USA. Both samples were crushed using a pulverizer and agate mortar and pestle. Selected size fractions of this powder were then cleaned ultrasonically using acetone. The resulting tremolite powders were

TABLE 1. Compositions, surface areas and size fractions of tremolite powders used in the present study.

Tremolite sampling locality	Abbreviation	Composition[a]	Size fraction (μm)	BET surface area (cm^2/g)[b]	Geometric surface area (cm^2/g)[c]
Felch, MI, USA	A	$Ca_{1.99}Mg_{5.02}Si_8O_{22}(OH)_2$	50–200	6409	147
Cannan, CT, USA	B1	$Ca_{2.10}Mg_{4.97}Fe_{0.07}Si_8O_{22}(OH)_2$	50–200	1057	147
Cannan, CT, USA	B2	$Ca_{2.10}Mg_{4.97}Fe_{0.07}Si_8O_{22}(OH)_2$	200–500	504	60

[a] Based on 8 Si in the structural formula (see text).
[b] The uncertainty in these measurements is estimated to be ±10%
[c] Calculated using equations reported by Wolff-Boenisch *et al*. (2004) adopting a tremolite density of 3.05 g/cm^3 and assuming that all grains were identically sized spheres having a diameter equal to the median of the indicated size fraction.

https://doi.org/10.1180/minmag.2014.078.6.12 Published online by Cambridge University Press

subsequently dried overnight at 110ºC. The mineralogy of these samples was analysed using an INEL CPS 120 X-ray diffractometer (XRD) using Co$K\alpha$ radiation, with a scan speed of 0.02º s^{-1}. Tremolite was the only phase evident in the XRD spectra. The elemental composition of these tremolites was determined using EDS spectroscopy. The resulting compositions were $Ca_{1.99}Mg_{5.02}Si_8O_{22}(OH)_2$ and $Ca_{2.10}Mg_{4.97}Fe_{0.07}Si_8O_{22}(OH)_2$, respectively, for tremolite A and B when normalized to 8 Si. The surface areas of the resulting tremolite powders, determined by the three-point BET method using a Quantachrome Autosorb-1 together with N_2 gas, are listed in Table 1. Images of the tremolite powders were taken prior to dissolution experiments using a JEOL 6360 LV Scanning Electron Microscope (SEM); some examples are shown in Fig. 1*a*,*b*. Prior to the dissolution experiments, the tremolite powder was free of fine particles and minerals other than tremolite.

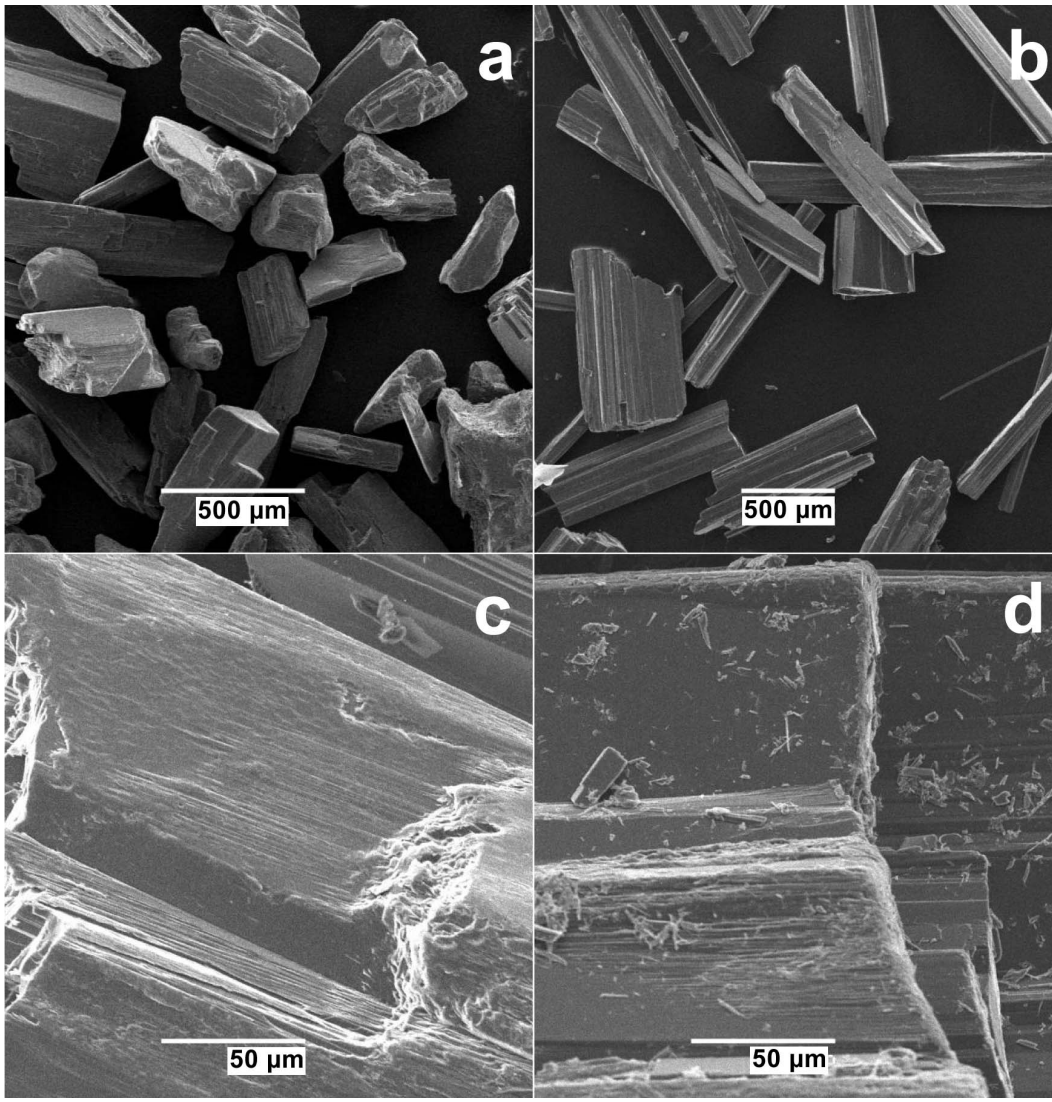

FIG. 1. Photomicrographs of (*a*) tremolite A and (*b*) tremolite B prior to the dissolution experiments, and of (*c*) tremolite B following its dissolution in experimental series B2-f and (*d*) tremolite A following its dissolution in experimental series A-a.

https://doi.org/10.1180/minmag.2014.078.6.12 Published online by Cambridge University Press

Two distinct open-system reactor systems were used in this study. Experiments were performed at 25, 37 and 50ºC in 250 ml Azalon plastic mixed-flow reactors placed in a thermostated bath (see Chairat *et al*., 2007). These reactors were fitted with Nalgene tubes for supply and recovery of experimental fluids, which were pumped through the reactor with Gilson peristaltic pumps. The reacted fluids were passed through a 0.45 μm Millipore Nitrocellulose in-line filter upon exiting the reactor. Floating teflon-coated stir bars were used to mix the powder/fluid mixture in the reactor and to avoid grinding. Experiments were performed at 80, 100 and 150ºC in a Parr titanium mixed-flow reactor system, such as described by Oelkers *et al*. (2008*b*). A High Precision/High Pressure Liquid Chromatography Pump provided continuous fluid flow ranging from 1 to 2 g/min during the experiments. The precision of the fluid flow rates was ±4%. The volume of the titanium reactor was 250 ml. The fluid within the reactor was stirred using a Parr magnetically driven stirrer, the temperature controlled by a Parr controlled furnace, and elevated pressure was maintained using a back-pressure regulator.

Experiments were performed in this study either individually or in series, consisting of several experiments performed on a single tremolite powder. Each experimental series is distinguished by the first two entries of its experiment number; the first entry indicates the identity of the tremolite powder used, and the second letter the experimental series run with this powder. For example, series A-a, was performed using tremolite A and consists of experiments A-a-1, A-a-2, and A-a-3. Note that some series consisted of just one experiment. At the beginning of each experimental series the reactor was dismantled at ambient conditions. A specific mass of tremolite powder was placed in the reactor. The reactor was filled with the initial inlet fluid, closed, and placed in a thermostated bath or in a furnace. The temperature, pressure, fluid flow, and stirring rate were adjusted to desired settings. The fluid flow rate and outlet fluid composition were measured regularly. After steady state was verified with a minimum of three constant Si concentrations in the outlet fluid samples obtained over several residence times (defined as the volume of the reactor divided by the reactive fluid flow rate): either (1) the experimental series was stopped; or (2) the inlet fluid composition, fluid flow rate and/or the temperature were then changed to the next desired experimental condition.

Dissolution experiments were performed in fluids consisting of demineralized H_2O, and reagent-grade HCl, NaCl, $CaCl_2$ and $MgCl_2$ from Merck, and aqueous SiO_2 created from the dissolution of amorphous SiO_2 at 80ºC. All inlet fluids had stoichiometric ionic strengths of 0.02 or 0.12 mol kg^{-1}. The compositions of all inlet fluids are listed in Table 2. Calcium and magnesium compositions of the inlet and outlet fluids were determined using a Perkin Elmer Zeeman 5000 atomic absorption spectrometer. Silica compositions were measured using the Molybdate Blue method (Koroleff, 1976). The reproducibility of chemical analyses was ±4% for Si, Mg and Ca concentrations >0.5, >0.1 and >0.1 ppm, respectively, but as much as ±10% at lower concentrations. Outlet fluid pH was measured at 25ºC immediately after sampling. All outlet fluids were undersaturated with respect to all possible secondary phases as confirmed by *PHREEQC* calculations.

Steady-state forward dissolution rates (r_+) were computed from the measured steady-state solution compositions using

$$r_+ = \frac{\Delta m_i F}{\nu_i \bar{s}_{\mathrm{BET}} M} \qquad (10)$$

where Δm_i stands for the concentration difference between the inlet and outlet of the ith element in solution, F represents the fluid mass flow rate, ν_i refers to the stoichiometric number of moles of the ith element in one mole of tremolite, and $\bar{s}_{\mathrm{BET}}$ denotes the BET specific surface area of the initial tremolite, and M signifies the initial mass of tremolite in the reactor.

Results

Photomicrographs of the tremolite surfaces following their dissolution during two representative experiments are shown in Fig. 1*c,d*. Two observations are apparent. First, dissolution appears to occur primarily on the tremolite prism edges, where the divalent cations can readily move out of the structure. Secondly, a significant number of fine-grained needle-shaped particles are present on the surfaces following the experiments.

Thirty four steady-state dissolution rates were obtained in this study; experimental results and conditions are summarized in Table 3. Two examples of the temporal evolution of instantaneous rates generated from Si, Mg and Ca release are shown in Fig. 2. The first example illustrates

https://doi.org/10.1180/minmag.2014.078.6.12 Published online by Cambridge University Press

TABLE 2. Summary of the initial conditions of the experiments performed in this study.

Temp (ºC)	Outlet pH	Exp. No.	Powder mass (g)	Ionic strength (mol/kg)	Inlet fluid composition (mol/kg)				
					HCl	NaCl	SiO_2	$MgCl_2$	$CaCl_2$
25	2.0	A-a-1	1.53	*0.02*	1.13×10^{-2}	8.70×10^{-3}			
37	2.0	A-a-2	1.53	*0.02*	1.13×10^{-2}	8.70×10^{-3}			
37	2.0	B2-a-1	3.11	0.02	1.13×10^{-2}	8.70×10^{-3}			
37	2.0	B2-a-2	3.11	0.12	1.23×10^{-2}	1.08×10^{-1}			
37	6.8	B2-b-1	3.05	0.02	2.0×10^{-5}	1.20×10^{-1}			
37	6.0	B2-b-2	3.05	0.12	2.0×10^{-5}	1.20×10^{-1}			
37	5.3	B2-c-1	3.06	0.02	2.0×10^{-5}	1.20×10^{-1}			
37	3.0	B2-c-2	3.06	0.12	1.22×10^{-3}	1.19×10^{-1}			
37	6.9	B2-d-1	3.12	0.12	2.0×10^{-5}	1.20×10^{-1}			
37	6.7	B2-e-1	3.21	0.12	2.0×10^{-5}	1.20×10^{-1}			
37	4.1	B2-f-1	2.94	0.12	1.22×10^{-4}	1.20×10^{-1}			
37	4.1	B2-g-1	2.98	0.12	1.22×10^{-4}	1.20×10^{-1}			
37	1.9	B2-h-1	3.05	0.12	1.23×10^{-2}	1.08×10^{-1}			
50	2.0	A-a-3	1.53	*0.02*	1.13×10^{-2}	8.70×10^{-3}			
50	2.0	B2-a-3	3.11	0.12	1.23×10^{-2}	1.08×10^{-1}			
50	4.1	B2-g-2	2.98	0.12	1.22×10^{-4}	1.20×10^{-1}			
50	2.0	B1-s-5	3.04	0.12	1.23×10^{-2}	1.08×10^{-1}	8.5×10^{-6}		
50	2.0	B1-s-6	3.04	0.12	1.23×10^{-2}	1.08×10^{-1}	1.5×10^{-5}		
50	2.0	B1-s-7	3.04	0.12	1.23×10^{-2}	1.08×10^{-1}	1.6×10^{-4}		
50	1.9	B2-h-2	3.05	0.12	1.23×10^{-2}	1.08×10^{-1}			
50	2.0	B1-a-1	3.04	0.12	1.23×10^{-2}	1.08×10^{-1}			
50	4.1	B2-f-2	2.94	0.12	1.22×10^{-4}	1.20×10^{-1}			
50	2.0	B1-a-2	3.04	0.12	1.23×10^{-2}	1.08×10^{-1}		3.5×10^{-5}	
50	2.0	B1-a-3	3.04	0.12	1.23×10^{-2}	1.08×10^{-1}		1.4×10^{-4}	
50	2.0	B1-a-4	3.04	0.12	1.23×10^{-2}	1.08×10^{-1}		9.0×10^{-4}	
50	6.1	B2-b-3	3.05	0.12	2.0×10^{-5}	1.20×10^{-1}			
50	3.1	B2-c-3	3.06	0.12	1.22×10^{-3}	1.19×10^{-1}			
50	2.0	B1-a-8	3.04	0.12	1.23×10^{-2}	1.08×10^{-1}			1.8×10^{-4}
80	4.5	B2-j-1	3.19	0.12	1.5×10^{-4}	1.20×10^{-1}			
80	2.2	B2-k-1	1.06	0.12	1.23×10^{-2}	1.08×10^{-1}			
100	4.4	B2-j-2	3.19	0.12	1.5×10^{-4}	1.20×10^{-1}			
100	2.0	B2-k-2	1.06	0.12	1.23×10^{-2}	1.08×10^{-1}			
150	4.4	B2-j-3	3.19	0.12	1.5×10^{-4}	1.20×10^{-1}			
150	2.0	B2-k-3	1.06	0.12	1.23×10^{-2}	1.08×10^{-1}			

TABLE 3. Summary of the results of all experiments performed in the present study.

Temp (°C)	pH	Exp. no.	Surface area (cm^2)[a]	Flow rate (g/min)	Outlet fluid concentrations (mol/kg × 10^6)			$Log(a^2_{H^+}/a_{Mg^{2+}})$	– Log ($r_{+,i}$/(mol/cm^2/s)) –			Log (SI) Tremolite[b]
					Si	Mg	Ca		Si	Mg	Ca	
T = 25	2.0	A-a-1	9821	0.083	9.1	6.9	16	1.40	−15.79	−15.71	−14.95	−110.30
T = 37	2.0	A-a-2	9821	0.091	23	14	20	1.11	−15.35	−15.38	−14.81	−102.69
	2.0	B2-a-1	1555	0.018	27	29	25	0.77	−15.18	−14.94	−14.62	−100.24
	2.0	B2-a-2	1555	0.018	17	16	15	1.20	−15.38	−15.22	−14.83	−104.78
	6.8	B2-b-1	1525	0.019	1.1	Bd	Bd	−7.08	−16.56	–	–	−56.99
	6.0	B2-b-2	1525	0.018	1.2	Bd	Bd	−5.31	−16.54	–	–	−69.08
	5.3	B2-c-1	1530	0.017	1.0	12	Bd	−5.46	−16.61	−15.35	–	−71.22
	3.0	B2-c-2	1530	0.018	6.4	5.0	7.2	−0.31	−15.81	−15.71	−15.16	−97.26
	6.9	B2-d-1	1560	0.018	5.1	13	27	−8.21	−15.92	−15.32	−14.59	−40.34
	6.7	B2-e-1	1605	0.016	5.0	15	19	−8.19	−15.99	−15.31	−14.80	-43.13
	4.1	B2-f-1	1470	0.017	4.2	2.7	6.1	−2.24	−16.00	−15.99	−15.23	−84.83
	4.1	B2-g-1	1490	0.018	7.8	4.2	5.5	−2.44	−15.71	−15.78	−15.26	−81.80
	1.9	B2-h-1	1525	0.017	11	6.9	10	1.75	−15.58	−15.58	−15.01	−109.79
T = 50	2.0	A-a-3	9821	0.351	18	11	18	1.22	−14.06	−14.90	−14.27	−101.36
	2.0	B2-a-3	1555	0.019	47	35	20	0.85	−14.92	−14.84	−14.69	−96.45
$[Si]_{inlet}$ M	4.1	B2-g-2	1490	0.017	15	8.7	11	−2.74	−15.45	−15.47	−14.97	−74.62
8.5E-06	2.0	B1-s-5	3217	0.081	16	8.0	14	1.50	−15.38	−15.17	−14.52	−103.61
1.5E-05	2.0	B1-s-6	3217	0.075	24	7.9	15	1.50	−15.38	−15.21	−14.55	−102.30
1.6E-04	2.0	B1-s-7	3217	0.076	180	7.6	13	1.52	−15.11	−15.22	−14.60	−95.55
	1.9	B2-h-2	1525	0.017	29	21	14	1.28	−15.16	−15.11	−14.89	−101.00
	2.0	B1-a-1	3217	0.077	10	7.9	19	1.50	−15.28	−15.20	−14.42	−104.94
$[Mg]_{inlet}$ M	4.1	B2-f-2	1470	0.017	9.8	6.1	9.2	−2.59	−15.64	−15.64	−15.06	−76.96
3.5E-05	2.0	B1-a-2	3217	0.127	5.8	39	13	0.81	−15.32	−15.37	−14.38	−103.89
1.4E-04	2.0	B1-a-3	3217	0.125	6.1	140	13	0.24	−15.31	−15.27	−14.38	−100.86
9.0E-04	2.0	B1-a-4	3217	0.125	6.0	330	14	−0.12	−15.31	–	−14.35	−99.03
	6.1	B2-b-3	1525	0.018	3.3	Bd	Bd	−5.98	−16.07	–	–	−55.65
$[Ca]_{inlet}$ M	3.1	B2-c-3	1530	0.021	21	13	9.4	−0.93	−15.23	−15.22	−14.97	−86.63
1.8E-04	2.0	B1-a-8	3217	0.123	5.9	4.7	180	1.73	−15.33	−15.23	−14.74	−106.12
T = 80	4.5	B2-j-1	1595	0.974	7.9	5.0	3.5	−3.28	−14.00	−13.99	−13.74	−67.45
	2.2	B2-k-1	530	1.043	6.7	4.2	5.9	1.41	−13.56	−13.56	−13.01	−100.18

T = 100	4.4	B2-j-2	1595	1.007	17	11	4.9	−3.39	−13.64	−13.65	−13.59	−60.6
	2.0	B2-k-2	530	0.988	32	20	12	1.16	−12.91	−12.92	−12.75	−90.12
T = 150	4.4	B2-j-3	1595	1.016	74	45	17	−3.92	−13.01	−13.02	−13.05	−43.9
	2.0	B2-k-3	530	1.987	310	200	82	0.24	−13.77	−13.76	−13.74	−67.95

[a] Initial surface area of tremolite powder present in the reactor
[b] Log of the saturation index of the steady-state outlet fluid with respect to tremolite as calculated using *PHREEQC*.

rates during experimental series B2-g, performed at pH 4.3 and temperatures of 37 and 50ºC. The initial release rates of both Mg and Ca are approximately an order of magnitude faster than that of Si after normalization to the stoichiometry of the dissolving tremolite. The release rates of Mg decrease with time to be stoichiometric with respect to Si after ~25 days of elapsed time, and remain near to stoichiometric with respect to Si until the end of the experimental series. In contrast, the Ca release rates remain ~0.6 orders of magnitude faster until the end of this series. The second example illustrates the instantaneous tremolite dissolution rates in experiment B2-e-1 performed at pH 6.9 at a temperature of 37ºC. Initially, Mg and Si are released in stoichiometric

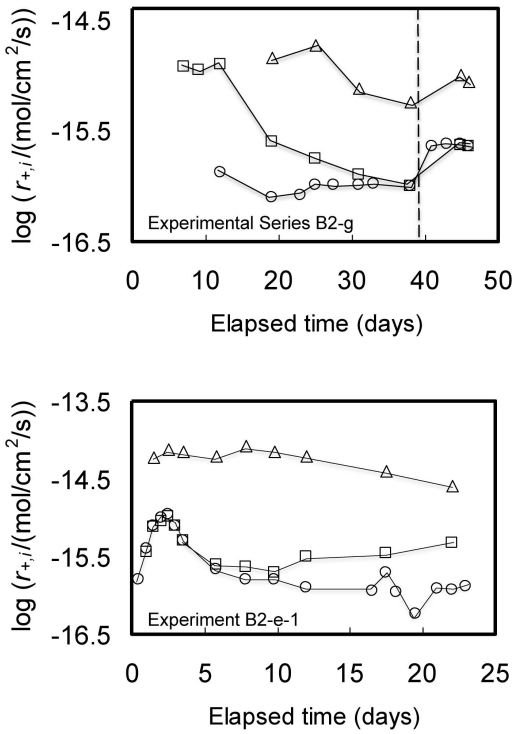

FIG. 2. Temporal evolution of instantaneous tremolite dissolution rates based on Ca, Mg and Si release during experimental series B2-g, performed at pH 4.3 and experiment B2-e-1, performed at pH 6.9. In both cases the inlet fluids were Si-, Mg- and Ca-free. The open circles, squares and triangles correspond to rates calculated based on Si, Mg and Ca release, respectively. The dashed vertical line in the upper part of the figure indicates the time at which the reactor temperature was changed from 37 to 50ºC.

https://doi.org/10.1180/minmag.2014.078.6.12 Published online by Cambridge University Press

proportions, with Ca being released more than an order of magnitude faster. As Si release rates approach steady state, the Mg release rate appears to increase and its release rates are ~0.3 orders of magnitude greater than that of Si at the end of the experiment.

The logarithms of steady-state tremolite dissolution rates based on Mg and Ca release are compared with those based on Si release in Fig. 3. Note that the definition of steady state adopted in this study is that of a near constant Si release rate; Mg and Ca may not have attained a steady-state in these experiments. Nevertheless, as can be seen in Fig. 3, tremolite dissolution rates based on Mg release generally fall within 0.3 log units of the corresponding Si rates. In contrast, steady-state rates based on Ca release are, on average, six times greater than corresponding rates based on Si release. Note that rates based on Ca release measured at the elevated temperature are closer to or even lower than their corresponding Si rates determined at temperatures >80ºC

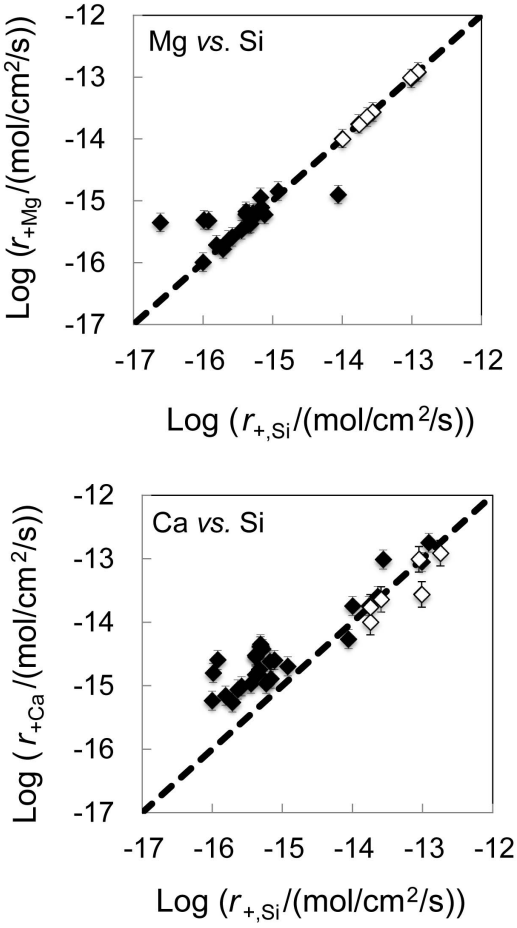

FIG. 3. Logarithms of measured forward steady-state tremolite dissolution rates based on Mg and Ca release plotted as a function of the corresponding rates based on Si release. The symbols represent all the rates determined in this study whereas the dashed lines correspond to equal values of the plotted rates. Filled and open symbols illustrate rates measured at temperatures below and equal to or greater than 80ºC, respectively. The error bars are consistent with a ±0.15 uncertainty in the rates.

The variation of forward steady-state tremolite dissolution rates measured at 37 and 50ºC based on Si release are depicted as a function of pH in Fig. 4 and as a function of $\log(a^2_{H^+}/a_{Mg^{2+}})$ in Fig. 5. The general trend of the rates is to decrease with increasing pH with a log rate *vs.* pH slope near −0.25. Similarly, despite scatter, rates tend to increase with increasing $\log(a^2_{H^+}/a_{Mg^{2+}})$; the dashed lines drawn in Fig. 5, consistent with the symbols, have a slope of 0.125, consistent with $n = 8$ in equation 7.

The variation of measured steady-state tremolite dissolution rates at pH ~2 as a function of temperature are quantified in the present study using the empirical Arrhenius equation, equation 8. The activation energy and pre-exponential constant in equation 9 were obtained with the aid of the plot shown in Fig. 6.

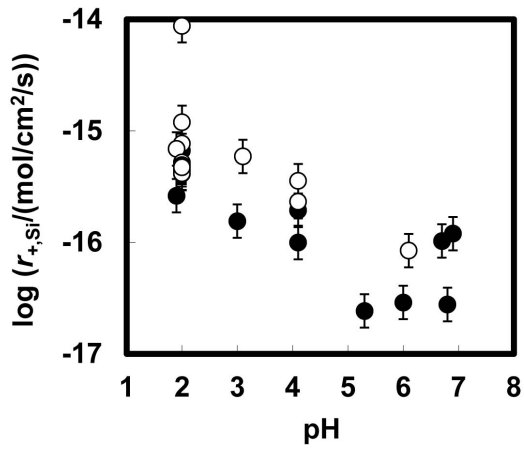

FIG. 4. Logarithms of measured forward steady-state tremolite dissolution rates as a function of pH. Filled and open symbols represent rates measured at 37 and 50ºC, respectively. The error bars are consistent with a ±0.15 uncertainty in the rates. The error bars are consistent with a ±0.15 uncertainty in the rates.

https://doi.org/10.1180/minmag.2014.078.6.12 Published online by Cambridge University Press

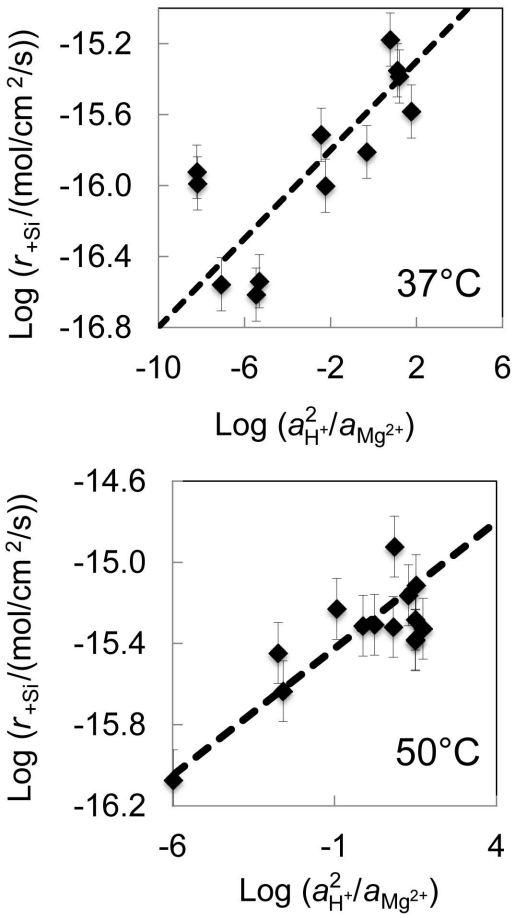

FIG. 5. Logarithms of forward steady-state tremolite dissolution rates depicted as a function of $\log(a^2_{H^+}/a_{Mg^{2+}})$ at 37 and 50ºC. The dashed lines have slopes of 1/8. The error bars are consistent with a ±0.15 uncertainty in the rates.

Regression of these data, as illustrated in this figure, yields E_A = 80 kJ/mol.

The distribution of rates and the curves shown in Figs 5 and 6 suggest that tremolite steady-state dissolution rates can be described as a function of temperature and fluid composition using

$$r_+ = (6 \times 10^{-4}\ \text{mol/cm}^2\text{/s}) e^{-\left(\frac{80\ \text{kJ/mol}}{RT}\right)} \left(\frac{a^2_{H^+}}{a_{Mg^{2+}}}\right)^{1/8} \quad (11)$$

The degree to which equation 11 describes the rate obtained in the present study can be assessed

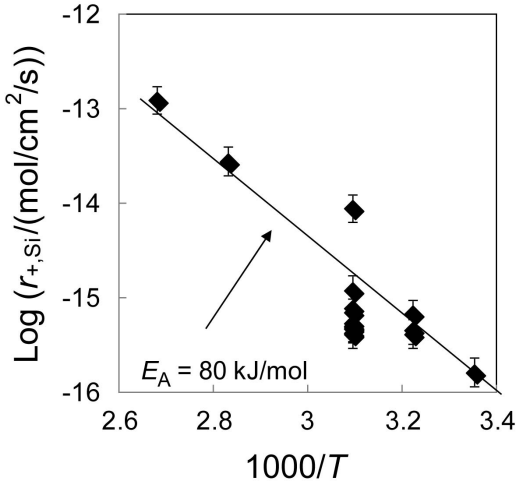

FIG. 6. Logarithm of all forward steady-state tremolite dissolution rates determined in this study at pH 2 as a function of 1000 times reciprocal absolute temperature. The line passing through the data points is consistent with an activation energy of 80 kJ/mol.

with Fig. 7 which compares rates determined using equation 11 with their measured counterparts. The average difference between calculated and measured rates is 0.3 log units.

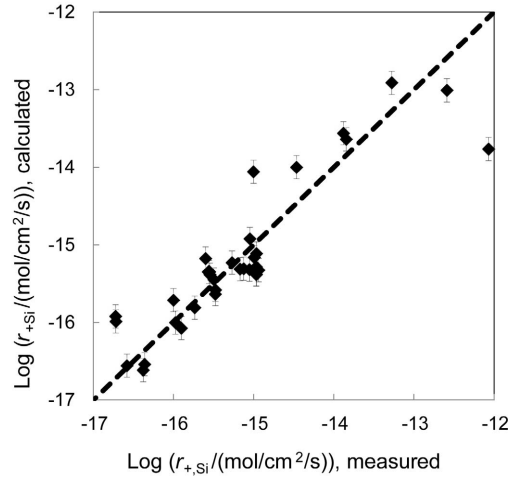

FIG. 7. Comparison of all forward steady-state tremolite dissolution rates measured in this study with those calculated using equation 11. The symbols represent measured and calculated rates, whereas the dashed line corresponds to equal values of these two rates. The error bars are consistent with a ±0.15 uncertainty in the rates.

https://doi.org/10.1180/minmag.2014.078.6.12 Published online by Cambridge University Press

Discussion

Calcium release and tremolite toxicity

The preferential release of Ca has been observed throughout all experiments performed at T<80ºC. Similar to the behaviour of wollasonite during its dissolution (Schott *et al*. 2012), Ca appears to be removed more quickly than and independently of the other elements. In the case of wollastonite, the Ca-depleted layer does not attain a steady-state thickness at acidic conditions, but grows continuously. Such also appears to be the case for tremolite at least for the duration of the <80ºC experiments; the tremolite structure has channels parallel to its Si tetrahedral chains allowing for the ready removal of Ca through proton-exchange reactions.

A significant observation is that the tremolite structure consists of linear talc-like Mg-Si ribbons, with the Mg in 6-fold coordination bound together by adjoining Ca in 8-fold coordination (Warren, 1930; Hawthorne and Oberti, 2007). A schematic illustration of the tremolite structure, projected down its *c* axis is shown in Fig. 8. It is clear from this image that the removal of Ca will liberate the talc-like ribbons from the bulk tremolite, creating fine needle-like particles. Such particles are evident from the tremolite recovered following the dissolution experiments performed in the present study. It follows that the preferential Ca release in lung fluids could promote the toxicity of inhaled tremolite through the creation of such fine-grained needle-like particles.

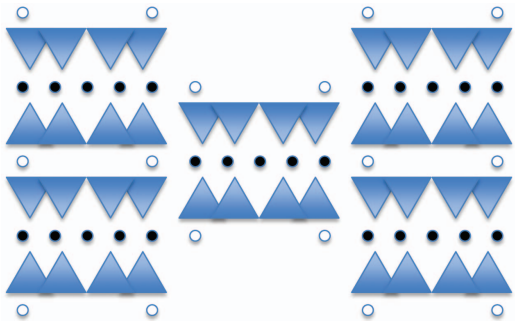

FIG. 8. Schematic drawing showing a projection of the tremolite structure down the *c* axis (after Bozhilov and Jenkins, 2007). The structure consists of blue Si–O tetrahedral units in double chains oriented parallel to the *a* and *b* axes. These chains are bound together in talc-like strips by 6-coordinated Mg atoms, shown as black circles. These talc-like strips are then bound in tremolite by 8-coordinated Ca atoms shown as open circles.

Comparison of the dissolution rates of Mg-silicate minerals

The dissolution rates of selected Mg-silicate minerals at ambient temperatures are illustrated in Fig. 9. The rates shown were selected because they were all generated using similar techniques in the same laboratory, facilitating their comparison. Mg-silicate dissolution rates all tend to decrease with increasing pH, though there is some indication that these rates become pH independent at alkaline conditions. Notably, the dissolution rates decrease substantially with the degree of connectiveness of the Si structure. Forsterite, consisting of isolated Si tetrehedra, dissolves faster than enstatite, which is made up of single chains of Si tetrehedra, which itself dissolves faster than talc and tremolite, consisting of sheets of Si tetrehadra, and talc-like double-chained Si tetrehedra. The similar talc and tremolite dissolu-

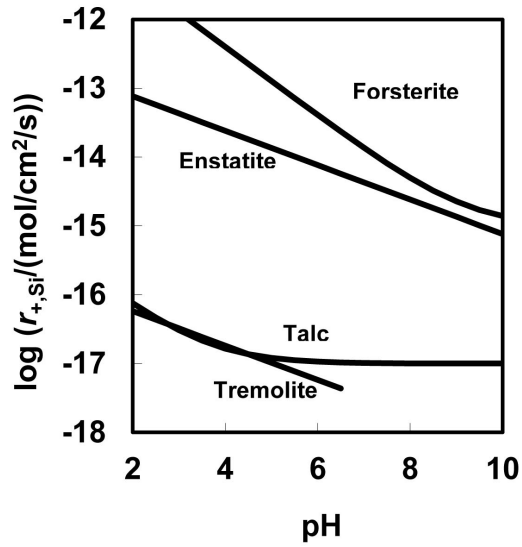

FIG. 9. Comparison of 25ºC forward steady-state dissolution rates as a function of pH for selected Mg-silicate minerals (after Schott *et al.*, 2009) and an aqueous Mg^{2+} activity of 1×10^{-4}. Rates for talc and enstatite were calculated using equations reported by Saldi *et al*. (2007) and Oelkers and Schott (2001), whereas those for forsterite were reported by Pokrovsky and Schott (2000). Rates for tremolite were calculated using equation 11.

https://doi.org/10.1180/minmag.2014.078.6.12 Published online by Cambridge University Press

tion rates probably reflect the similarity in their Si-Mg-O framework after the Ca is removed from the latter mineral. Taken together, the comparison shown in Fig. 9 is consistent with a similar dissolution mechanism for these minerals comprising the relatively fast removal of Mg followed by the slower rate-limiting liberation of partially detached Si from the mineral surface.

Experimental uncertainties and data scatter

Uncertainties associated with the rates generated in this study arise from a variety of sources, including the measurement of aqueous solution concentrations, fluid-flow rates, and tremolite surface areas. The uncertainties in the measured values of total aqueous silica, magnesium, and calcium concentration are on the order of ±10% or less. Computational and experimental uncertainties in the pH measured are on the order of ±0.04 pH units. Uncertainties in fluid-flow rate measurements are not more than 4%. The uncertainty associated with the measurement of the surface area of the initial tremolite powder is ±10%. If uncertainties were estimated exclusively from the sum of these contributions, an overall uncertainty of the dissolution rates reported would be of the order of 20%. Nevertheless it is clear from Figs 4–6 that other sources lead to the additional scatter in the measured rates. According to mass-balance calculations, <5% of the initial tremolite powder was dissolved in any experimental series. It seems possible, however, that the tremolite surface area present in the reactor evolves significantly during the experiments. Although post-experiment surface areas were not measured, as emphasized above, a significant number of fine, needle-shaped gains were formed during the dissolution experiments performed in this study. As emphasized by a number of studies (Gautier *et al*., 1994; Luttge *et al*., 2013; Fischer *et al*., 2014), the degree to which reactive surface area varies in response to dissolution is currently impossible to define unambiguously, yet consideration of the scatter in the Figs 4–6 suggests that such effects may be large. This conclusion is consistent with the rates obtained from experimental series A-a, which dissolved tremolite at pH 2 and 25, 37 and 50ºC. This experimental series leads to an anomalously fast rate during the third experiment performed in the series, after it had already dissolved at pH 2 at 25 and 37ºC, potentially due to the creation of fine particles related to the preferential release of Ca.

Conclusions

The results and discussion presented above illustrate the distinct dissolution behaviour of tremolite. Tremolite dissolution rates based on Si or Mg release are orders of magnitude slower than corresponding dissolution rates of forsterite and enstatite. As a consequence, the carbonation of tremolite will be far less efficient than the carbonation of these other Mg silicate minerals, limiting its potential in mineral carbon storage efforts. The dissolution of tremolite, however, releases calcium preferentially, at least at temperature >80ºC. This preferential release continues for a substantial amount of time, leading to the extensive removal of Ca from the tremolite surface. Due to its mineral structure, the removal of Ca will promote the breaking apart of the tremolite into small needle-shaped particles, which probably will increase its toxicity to human lungs. It seems, therefore, that an improved understanding of the chemical processes controlling the retention *vs*. the removal of Ca may help to design methods to limit the toxicity of this mineral.

Acknowledgements

The authors thank Alain Castillo for technical assistance throughout the duration of the experimental work, Carole Causserand for her generous help during the analytical part of the work, and Philippe de Parseval for his assistance with the SEM images. They also thank Stacey Callahan, Oleg Pokrovsky, Pascale Bénézeth, Chris Pearce, Julian Declercq and Morgan T. Jones for helpful discussions during the course of this study. Support from Centre National de la Recherche Scientifique, and the National Science Foundation is gratefully acknowledged.

References

Aagaard, P. and Helgeson, H.C. (1977) Thermodynamic and kinetic constraints on the dissolution of feldspars. *Geological Society of America Abstracts with Program*, **9**, 873.

Aagaard, P. and Helgeson, H.C. (1982) Thermodynamic and kinetic constraints on reaction rates among minerals and aqueous solutions: I. Theoretical considerations. *American Journal of Science*, **282**, 237–285.

Addison, J. and McConnell, E.E. (2008) A review of carcinogenicity studies of asbestos and non-abestos

https://doi.org/10.1180/minmag.2014.078.6.12 Published online by Cambridge University Press

tremolite and other amphiboles. *Regulatory Toxicology and Pharmacology*, **52**, S187–S199.

Arrhenius, S. (1889) Über die Reaktionsgeschwindigkeit bei der Inversion von Rohzucker durch Säuren. *Zeitschrift für physikalische Chemie*, **4**, 226–248.

Berner, R.A. and Schott, J. (1982) Mechanism of pyroxene and amphibole weathering. 2. Observations of soil grains. *American Journal of Science*, **282**, 1214–1231.

Bozhilov, K.N. and Jenkins, D.M. (2007) Analytical electron microscopy of tremolite. Pp. 616–625 in: *Modern Research and Educational Topics in Microscopy*, vol. **2** (A. Mendez-Vilas and J. Dias, editors). Formatex.

Brantley, S.L. and Chen, Y. (1995) Chemical weathering rates of pyroxenes and amphiboles. Pp. 119–172 in: *Chemical Weathering Rates of Silica Minerals* (A.F. White and S.L. Brantley, editors). Reviews in Mineralogy, **31**, Mineralogical Society of America, Washington, D.C.

Case, B.W. (1991) Health effects of tremolite. Pp. 491–504 in: *The Third Wave of Asbestos Disease: Exposure to Asbestos in Place* (P.J. Landrigan and H. Kazemi, editors). Annals of the New York Academy of Sciences, **643**.

Chaïrat, C., Schott, J., Oelkers, E.H., Lartigue J.-E. and Harouiya, N. (2007) Kinetics and mechanism of natural fluorapatite dissolution at 25ºC and pH from 3 to 12. *Geochimica et Cosmochimica Acta*, 7**1**, 5901–5912.

Chen, Y. and Brantley, S.L. (1998) Diopside and anthopyllite dissolution at 25ºC and 90ºC and acid pH. *Chemical Geology*, **147**, 233–248.

Churg, A. (1988) Chrysotile, tremolite, and malignant mesothelioma in man. *Chest*, **93**, 621–628.

Daval, D., Hellmann, R., Crovisier, J., Tisserand, D., Martinez, I. and Guyot, F. (2011*a*) Dissolution kinetics of diopside as a function of solution saturation state: Macroscopic measurements and implication for modeling of geologic storage of CO_2. *Geochimica et Cosmochimica Acta*, **74**, 2615–2633.

Daval, D., Sissmann, O., Menguy, N., Saldi, G.D., Guyot, F., Martinez, I., Crovixier, J., Garcia, B., Machouk, I., Knauss, K. and Hellmann, R. (2011*b*) Influence of amorphous silica layer formation on the dissolution rate of olivine at 90ºC and elevated pCO_2. *Chemical Geology*, **284**, 193–209.

Daval, D., Hellmann, R., Saldi, G.D., Wirth, R. and Knauss, K. (2013) Linking mm-scale measurements of the anisotropy of silicate surface reactivity to macroscopic dissolution rate laws: New insights based on diopside. *Geochimica et Cosmochimica Acta*, **107**, 121–134.

Davis, J.A. and Kent, D.B. (1990) Surface complexation in aqueous solutions. Pp. 177–260 in: *Mineral–Water Interface Geochemistry* (M.F. Hochella and A.F. White, editors). Reviews in Mineralogy, **23**, Mineralogical Society of America, Washington, D.C.

Davis, J.M.G., Addison, J., McIntosh, C., Miller, B.G. and Niven, K. (1991) Variations in the carcinogenicity of tremolite dust samples of differing morphology. Pp. 473–490 in: *The Third Wave of Asbestos Disease: Exposure to Asbestos in Place* (P.J. Landrigan and H. Kazemi, editors). Annals of the New York Academy of Sciences, **643**.

Dixit, S. and Carrroll, S.A. (2007) Effect of solution saturation state and temperature on diopside dissolution. *Geochemical Transactions*, **8**, 3.

Fischer, C., Kurganskaya, I., Schaefer, I., Schafer, T. and Luttge, A. (2014) Variability of crystal surface reactivity: What do we know? *Applied Geochemistry*, **43**, 132–157.

Gautier, J.-M., Oelkers, E.H. and Schott, J. (2001) Are quartz dissolution rates proportional to BET surface areas? *Geochimica et Cosmochimica Acta*, **65**, 1059–1070.

Gislason, S.R. and Oelkers, E.H. (2014) Carbon storage in basalt. *Science*, **344**, 373–374.

Golubev, S.V. and Pokrovsky, O.S. (2006) Experimental study of the effect of organic ligands on diopside dissolution kinetics. *Geochimica et Cosmochimica Acta*, **235**, 377–389.

Golubev, S.V., Pokrovsky, O.S. and Schott, J. (2005) Experimental determination of the effect of dissolved CO_2 on the dissolution kinetics of Mg and Ca silicates at 25ºC. *Chemical Geology*, **217**, 227–238.

Gunter, M.E., Belluso, E. and Mottana, A. (2007) Amphiboles: Environmental and health concerns. Pp. 453–516 in: *Amphiboles: Crystal Chemistry, Occurrence, and Health Issues* (F.C. Hawthorne, R. Oberti, G. Della Ventura and A. Mottana, editors). Reviews in Mineralogy and Geochemistry, **67**, Mineralogical Society of America, Chantilly, Virginia, USA and the Geochemical Society, St. Louis, Missouri, USA.

Hawthorne, F.C. and Oberti, R. (2007) Amphiboles: Crystal chemistry. Pp. 1–54 in: *Amphiboles: Crystal Chemistry, Occurrence, and Health Issues* (F.C. Hawthorne, R. Oberti, G. Della Ventura and A. Mottana, editors). Reviews in Mineralogy and Geochemistry, **67**, Mineralogical Society of America, Chantilly, Virginia, USA and the Geochemical Society, St. Louis, Missouri, USA.

Hänchen, M., Prigobbe, V., Baciocchi, R. and Mazzotti, M. (2008) Precipitation in the Mg-carbonate system – effects of temperature and CO_2 pressure. *Chemical Engineering Science*, **63**, 1012–1028.

Johnson, J.W., Anderson, G. and Parkhurst, D. (2000) Database from 'thermo.com.V8.R6.230' prepared at Lawrence Livermore National Laboratory,

https://doi.org/10.1180/minmag.2014.078.6.12 Published online by Cambridge University Press

(Revision: 1.11), California, USA.

Jurinski, J.B. and Rimstidt, J.D. (2001) Biodurability of talc. *American Mineralogist*, **86**, 392–399.

King, H.E., Plumper, O. and Putnis, A. (2010) Effect of secondary phase formation on the carbonation of olivine. *Environmental Science & Technology*, **44**, 6503–6509.

King, H.E., Satoh, H., Tsukamoto, K. and Putnis, A. (2014) Specific surface measurements of olivine dissolution by phase shift interferometry. *American Mineralogist*, **99**, 377–386.

Knauss, K.G., Nguyen, S.N. and Weed, H.C. (1993) Diopside dissolution kinetics as a function of pH CO_2, temperature and time. *Geochimica et Cosmochimica Acta*, **57**, 285–294.

Koroleff, F. (1976) Determination of silicon. Pp. 149–158 in: *Methods of Seawater Analysis* (K. Grasshoff, editor). Springer Verlag, New York.

Lasaga, A.C. (1981) Transition state theory. Pp. 135–169 in: *Kinetics of Geochemical Processes* (A.C. Lasaga and R.J. Kirkpatrick, editors). Reviews in Mineralogy, **8**, Mineralogical Society of America, Washington, D.C.

Lin, F.-C. and Clemency, C.V. (1981) The dissolution kinetics of brucite, antigorite, talc and phlogopite at room temperature and pressure. *American Mineralogist*, **66**, 801–806.

Luce, R.W., Bartlett, W.B. and Parks, G.A. (1972) Dissolution kinetics of magnesium silicates. *Geochimica et Cosmochimica Acta*, **36**, 35–50.

Luttge, A., Arvidson, R.S. and Fischer, C. (2013) A stochastic treatment of crystal dissolution kinetics. *Elements*, **9**, 183–188.

Mast, M.A. and Drever, J.I. (1987) The effect of oxalate on the dissolution rates of oligoclase and tremolite. *Geochimica et Cosmochimica Acta*, **51**, 2559–2568.

Murphy, W.M. and Helgeson, H.C. (1987) Thermodynamic and kinetic constraints on reaction rates among minerals and aqueous solutions. III. Activated complexes and the pH-dependence of the rates of feldspar, pyroxene, wollastonite, and olivine hydrolysis. *Geochimica et Cosmochimica Acta*, **51**, 3137–3153.

Murphy, W.M. and Helgeson, H.C. (1989) Thermodynamic and kinetic constraints on reaction rates among minerals and aqueous solutions. IV. Retrieval of rate constants and activation parameters for the hydrolysis of pyroxene, wollastonite, olivine, andalusite, quartz and nepheline. *American Journal of Science*, **289**, 17–101.

Oelkers, E.H. (2001*a*) General kinetic description of multioxide silicate mineral and glass dissolution. *Geochimica et Cosmochimica Acta*, **65**, 3703–3719.

Oelkers, E.H. (2001*b*) An experimental study of forsterite dissolution rates as a function of temperature and aqueous Mg and Si concentration. *Chemical Geology*, **175**, 485–494.

Oelkers, E.H. and Cole, D.R. (2008) Carbon dioxide sequestration: A solution to a global problem. *Elements* **4**, 305–310.

Oelkers, E.H. and Schott, J. (1998) Does organic acid adsorption affect alkali-feldspar dissolution rates? *Chemical Geology*, **151**, 235–245.

Oelkers, E.H. and Schott, J. (2001) An experimental study of enstatite dissolution rates as a function of pH, temperature, and aqueous Mg and Si concentration, and the mechanism of pyroxene/pyroxenoid dissolution. *Geochimica et Cosmochimica Acta*, **65**, 1219–1231.

Oelkers, E.H. and Schott, J. (2005) Geochemical aspects of CO_2 sequestration. *Chemical Geology*, **217**, 183–186.

Oelkers, E.H., Gislason, S.R. and Matter, J. (2008*a*) Mineral carbonation of CO_2. *Elements*, **4**, 333– 337.

Oelkers, E.H., Schott, J., Gauthier, J.-M. and Herrero-Roncal, T. (2008*b*) An experimental study of the dissolution rates of muscovite. *Geochimica et Cosmochimica Acta*, **72**, 4948–4961.

Oelkers, E.H. Golubev, S.V., Chaïrat, C., Pokrovsky, O.S. and Schott, J. (2009) The surface chemistry of multi-oxide silicates. *Geochimica et Cosmochimica Acta*, **73**, 4617–4634.

Olsen, A.A. and Rimstidt, J.D. (2008) Oxalate-promoted forsterite dissolution at low pH. *Geochimica et Cosmochimica Acta*, **72**, 1758–1766.

Oze, C and Solt, K. (2010) Biodurability of chrystolite and tremolite asbestos in simulated lung and gastric fluids. *American Mineralogist*, **95**, 825–831.

Parkhurst, D.L. and Appelo, C.A.J. (1999) User's guide to PHREEQC (Version 2) – A computer program for speciation, batch-reaction, one-dimensional transport, and inverse geochemical calculations. *U.S. Geological Survey Water Resources Report 99–4259.*

Petit, J.C., Della, M.G., Dran, J.C., Schott, J. and Berner, R.A. (1987) Mechanism of diopside dissolution from hydrogen depth profiling. *Nature*, **325**, 705–707.

Pokrovsky, O.S. and Schott, J. (2000) Kinetics and mechanisms of forsterite dissolution at 25ºC and pH from 1 to 12. *Geochimica et Cosmochimica Acta*, **64**, 3313–3325.

Prigiobbe, V., Costa, G., Baciocchi, R., Hänchen, M. and Mazzotti, M. (2009) The effect of CO_2 and salinity on olivine dissolution kinetics at 120ºC. *Chemical Engineering Science*, **15**, 3510–3515.

Pugnaloni, A., Giantomassi, F., Lucarini, G., Capella, S., Bloise, A., Di Primo, R. and Belluso, E. (2013) Cytotoxicity induced by exposure to natural and synthetic tremolite asbestos: An in vitro pilot study. *Acta Histochemica*, **115**, 100–112.

Robledo, R. and Mossman, B. (1999) Cellular and molecular mechanisms of asbestos-induced fibrosis.

https://doi.org/10.1180/minmag.2014.078.6.12 Published online by Cambridge University Press

Journal of Cellular Physiology, **180**, 158–166.

Roggli, V.L., Vollmer, R.T., Butnor, K.J. and Sporn, T.A. (2002) Tremolite and mesothelioma, *Annals of Occupational Hygiene*, **46**, 447–453.

Rosso, J.J. and Rimstidt, J.D. (2000) A high resolution study of forsterite dissolution rates. *Geochimica et Cosmochimica Acta*, **64**, 797–811.

Rozalen, M., Ramos, M.E., Huertas, F.J., Fiore, S. and Gervilla, F. (2013) Dissolution kinetics and biodurability of tremolite particles in mimicked lung fluids: Effect of citrate and oxalate. *Journal of Asian Earth Sciences*, **77**, 318–326.

Ryu, K.W., Lee, M.G. and Jang, Y.N. (2011) Mechanism of tremolite carbonation. *Applied Geochemistry*, **26**, 1251–1221.

Saldi, G.D., Kohler, S.J., Marty, N. and Oelkers, E.H. (2007) Dissolution rates of talc as a function of solution composition, pH and temperature. *Geochimica et Cosmochimica Acta*, **71**, 3446–3457.

Saldi, G.D., Schott, J., Pokrovsky, O.S., Gautier, Q. and Oelkers, E.H. (2012) An experimental study of magnesite precipitation rates at neutral to alkaline conditions and 100–200ºC as a function of pH, aqueous solution composition and chemical affinity. *Geochimica et Cosmochimica Acta*, **83**, 93–109.

Schott, J. and Oelkers, E.H. (1995) Dissolution and crystallization rates of silicate minerals as a function of chemical affinity. *Pure and Applied Chemistry*, **67**, 903–910.

Schott, J., Berner, R.A. and Sjoberg, E.L. (1981) Mechanism of pyroxene and amphibole weathering – I. Experimental studies of iron-free minerals. *Geochimica et Cosmochimica Acta*, **45**, 2123–2135.

Schott, J., Pokrovsky, O.S. and Oelkers, E.H. (2009) The link between mineral dissolution/precipitation kinetics and solution chemistry. Pp. 207–258 in: *Thermodynamics and Kinetics of Water–Rock Interaction* (E.H. Oelkers and J. Schott, editors). Reviews in Mineralogy and Geochemistry, **70**, Mineralogical Society of America, Chantilly, Virginia, USA and the Geochemical Society, St. Louis, Missouri, USA.

Schott, J., Pokrovsky, O.S., Spalla, O., Devreux, F., Gloter, A. and Mielczarski, J.A. (2012) Formation, growth and transformation of leached layers during silicate minerals dissolution: The example of wollastonite. *Geochimica et Cosmochimica Acta*, **98**, 259–281.

Warren, B.E. (1930) The structure of tremolite, $H_2Ca_2Mg_5(SiO_3)_8$ *Zeitschrift für Kristallographie*, **72**, 42–57.

Wogelius, R.A. and Walther, J.V. (1991) Olivine dissolution at 25ºC: Effects of pH, CO_2 and organic acids. *Geochimica et Cosmochimica Acta*, **55**, 943–954.

Wogelius, R.A. and Walther, J.V. (1992) Olivine dissolution kinetics at near-surface conditions. *Chemical Geology*, **97**, 101–112.

https://doi.org/10.1180/minmag.2014.078.6.12 Published online by Cambridge University Press